COLOR TRANSFORM BETWEEN IMAGE PAIR USING COVARIANCE CORRESPONDENCES OF LOCAL COLOR DISTRIBUTIONS

Yusuke Tatesumi, Keisuke Iwata, Keiichiro Shirai,
Shinshu Univ.

Masahiro Okuda
Univ. of Kitakyushu

ABSTRACT

In the guided filter that performs operations such as denoising and contrast correction with the help of a guide image, the positions of corresponding subjects need to be *completely aligned*, otherwise the misaligned regions in the output image are deteriorated by blur. In this paper, we propose a guided filter for images which include moving *dynamic regions*. Our filter uses correspondences of *local covariance matrices* instead of using the conventional pixel-to-pixel correspondences. In addition, we also propose a classification method to detect the dynamic regions by using the support vector machine. Combining two kinds of guided filters for static/dynamic regions, more natural resulting images are obtained.

***Index Terms*—** color transformation, guided filtering, local covariance, support vector machine, image composition

1. INTRODUCTION

When restoring images deteriorated by noise and saturation of intensity, the use of multiple images provides better results than restoration from a single image. As for methods that use multiple images, this paper deals with guided filtering (GF) [1–4] that uses a guide (or called guidance) image under a different photographic conditions. This GF has recently been applied to a variety of applications such as contrast correction [5] and stereo matching [6]. In particular, target applications of our GF described in this paper are denoising and tone mapping that can handle a set of input and guide images with different color and intensity [2, 4, 5].

In general, the color distribution of a local image region (patch, for simplicity) has a feature called a *color-line* [7], that is, its shape extends linearly due to shading, or spreads planarly due to a mixture of colors. In a corresponding pair of patches taken from the same scene in the input and guide images, but taken under different conditions (*e.g.*, a different white balance), the shapes of the two color distributions tend to be similar, and thus one distribution can be approximated by the rotated and shifted version of the other distribution. Utilizing this feature, the existing GFs [1–4] deal with the problem of obtaining a transform matrix that minimizes the transformation error in each patch. Specifically, at a target pixel i and its neighboring pixels j in a patch Ω_i, the local pixel colors of the guide image $\mathbf{I}_j \in R^3$ (such as RGB or YCbCr) are transformed by a patch-wise transform matrix $\mathbf{A}_i \in R^{3\times 3}$ and an offset vector $\mathbf{b}_i \in R^3$ to make them more like the local pixel colors of the input image $\mathbf{p}_j \in R^3$:

$$\arg\min_{\mathbf{A},\mathbf{b}} \sum_i \sum_{j\in\Omega_i} w_{ij}\Big(\|\mathbf{A}_i\mathbf{I}_j + \mathbf{b}_i - \mathbf{p}_j\|_2^2 + R\Big), \qquad (1)$$

where w_{ij} are weights introduced to remove outliers and R is a regularizer to guarantee the existence of solutions $\mathbf{A}_i$ and $\mathbf{b}_i$[1]. When applying this GF to moving *dynamic regions*, *e.g.*, rustling leaves and ruffling water surfaces, the transformation errors increase due to the misalignment of pixels $\mathbf{p}_j$ and $\mathbf{I}_j$. As a result, matrix norms decrease $\|\mathbf{A}_i\| \to 0$ to reduce errors, and the contrasts of transformed patches decrease: $\mathbf{A}_i\mathbf{I}_j \to \mathbf{0}$.

In this paper, to address the above mentioned problem, we propose a novel GF specialized to handle the dynamic regions. As for its practical implementation, patch colors are transformed so as to conform the two *covariance matrices* of a patch pair, because the shape of a color distribution is numerically representable by its covariance matrix. The covariance matrices are obtained from color distributions $\{\mathbf{p}_j\}$ and $\{\mathbf{I}_j\}$ independently. Thus the conventional pixel-to-pixel correspondences are not required in our method. However, as a trade-off of not using these correspondences, discolorations (unevenness of color) are prone to arise in the color transformation. Thus the image qualities in motionless *static regions* are inferior to those of our conventional GF [4].

Our previous GF [4] and the proposed one in this paper have advantages and disadvantages, depending on the amount of noise and object motion. To utilize the advantages of both methods, we aim to classify the static and the dynamic regions, and apply a more appropriate GF for each region. As for the classification method, due to the substantial difference in color and intensity between the input and guide image pair, existing methods for image/video processing are unfortunately not applicable. Instead, we focus on the matrix norms and transformation errors in (1) as the main cause of the blur arising in output images, and introduce a classification method using these features. Our method adopts the *support vector machine* (SVM) [11] as a two class classifier, and classifies the static/dynamic regions by using feature vectors obtained from the GF [4] for static regions. The classified dynamic regions are processed by our proposed GF, while the static regions are processed by the conventional GF [4].

2. COLOR TRANSFORMATION USING CORRESPONDENCES BETWEEN COVARIANCE MATRICES

The aim of the proposed GF for dynamic regions is to obtain a transform matrix $\mathbf{A}_i$ and an offset vector $\mathbf{b}_i$ set, which is the result of conforming the shapes of two color distributions of each patch pair. The shape of a color distribution is numerically represented by a covariance matrix, and we formulate the optimization problem using (1) with a constraint on the covariances:

$$\text{Eq.(1)} \quad \text{s.t.} \quad \text{cov}(\{\mathbf{A}_i\mathbf{I}_j + \mathbf{b}_i\}_j) = \text{cov}(\{\mathbf{p}_j\}), \qquad (2)$$

where the definitions of the variables are the same as for (1). Since there exist some solutions for $\mathbf{A}_i$ and $\mathbf{b}_i$ that satisfy the constraint

[1]Eq. (1) that represents the local linear model was introduced by [8] for image matting, and has been used in many applications [9, 10]. The problem described in this paper is specific to a case where $\mathbf{p}_j$ is explicitly known such as a guide image.

(described in Sec. 3), a solution that roughly minimizes (1) is selected. A covariance matrix $\mathrm{cov}(\{\mathbf{x}_j\}) \in R^{3\times 3}$ is calculated using

$$\mathrm{cov}(\{\mathbf{x}_j\}) = \frac{1}{\sum_j w_{ij}} \sum_{j\in\Omega_i} (\mathbf{x}_j - \overline{\mathbf{x}}_i)(\mathbf{x}_j - \overline{\mathbf{x}}_i)^T, \tag{3}$$

where $\overline{\mathbf{x}}_i = \frac{1}{\sum_j w_{ij}} \sum_{j\in\Omega_i} w_{ij}\mathbf{x}_j$ denotes a weighted mean, and w_{ij} are weights for removing outliers. The selection of the weights depends on the application. In the experiment shown in Sec. 5, we set them in the same way as [2], and omit a detailed discussion in this paper.

2.1. Solution for $\mathbf{b}_i$

Expanding (2) using (3), and substituting $\mathbf{I}'_j = \mathbf{I}_j - \overline{\mathbf{I}}_i$ and $\mathbf{p}'_j = \mathbf{p}_j - \overline{\mathbf{p}}_i$, we get

$$\begin{aligned} &\mathrm{cov}(\{\mathbf{A}_i\mathbf{I}'_j + \mathbf{b}_i\}) - \mathrm{cov}(\{\mathbf{p}'_j\}) \\ &= \mathbf{A}_i\Big(\frac{1}{\sum_j w_{ij}}\mathbf{I}'_j\mathbf{I}'^T_j\Big)\mathbf{A}_i^T - \Big(\frac{1}{\sum_j w_{ij}}\mathbf{p}'_j\mathbf{p}'^T_j\Big) \\ &= \mathbf{A}_i\mathrm{cov}(\{\mathbf{I}'_j\})\mathbf{A}_i^T - \mathrm{cov}(\{\mathbf{p}'_j\}). \end{aligned} \tag{4}$$

In this process, the offset vector $\mathbf{b}_i$ is eliminated, and unrelated to this equation. Instead, as a substitution, by differentiating (1) w.r.t. $\mathbf{b}$ and setting it zero, $\mathbf{b}_i = \overline{\mathbf{p}}_i - \mathbf{A}_i\overline{\mathbf{I}}_i$ is obtained. Further, substituting the obtained $\mathbf{b}_i$ into the affine transform $\mathbf{A}_i\mathbf{I}_j + \mathbf{b}_i$, we get $\mathbf{A}_i(\mathbf{I}_j - \overline{\mathbf{I}}_i) + \overline{\mathbf{p}}_i$ which is rewritable as $\mathbf{A}_i\mathbf{I}'_j + \overline{\mathbf{p}}_i$. Comparing $\mathbf{A}_i\mathbf{I}'_j + \overline{\mathbf{p}}_i$ and $\mathbf{A}_i\mathbf{I}'_j + \mathbf{b}_i$ in (4), identically we obtain

$$\mathbf{b}_i = \overline{\mathbf{p}}_i. \tag{5}$$

2.2. Solution for $\mathbf{A}_i$

The solution of $\mathbf{A}_i$ is linked to the *decorrelation* and *reconstruction* used in the principal component analysis (PCA).

First, the covariance matrices $\mathrm{cov}(\{\mathbf{I}'_j\})$ and $\mathrm{cov}(\{\mathbf{p}'_j\})$ are decomposed using singular value decomposition (SVD) as

$$\mathrm{cov}(\{\mathbf{I}'_j\}) = \mathbf{U}_i\mathbf{\Sigma}_i\mathbf{U}_i^T, \quad \mathrm{cov}(\{\mathbf{p}'_j\}) = \mathbf{V}_i\mathbf{\Xi}_i\mathbf{V}_i^T. \tag{6}$$

Then they are split into two matrices as

$$\mathbf{Q}_i\mathbf{Q}_i^T = (\mathbf{U}_i\mathbf{\Sigma}_i^{\frac{1}{2}})(\mathbf{\Sigma}_i^{\frac{1}{2}}\mathbf{U}_i^T), \quad \mathbf{R}_i\mathbf{R}_i^T = (\mathbf{V}_i\mathbf{\Xi}_i^{\frac{1}{2}})(\mathbf{\Xi}_i^{\frac{1}{2}}\mathbf{V}_i^T), \tag{7}$$

where $\mathbf{U} = [\mathbf{u}_1|\mathbf{u}_2|\mathbf{u}_3]$ and $\mathbf{V} = [\mathbf{v}_1|\mathbf{v}_2|\mathbf{v}_3] \in R^{3\times 3}$ (i is omitted for simplicity) are orthogonal matrices consisting of the 1st, 2nd, and 3rd principal axes of each color distribution, which are given by the eigenvectors of the covariance matrices. $\mathbf{\Sigma} = \mathrm{diag}(\sigma_1^2, \sigma_2^2, \sigma_3^2)$ and $\mathbf{\Xi} = \mathrm{diag}(\xi_1^2, \xi_2^2, \xi_3^2) \in R^{3\times 3}$ where $\sigma_k \geq \sigma_{k+1}$ and $\xi_k \geq \xi_{k+1}$ are diagonal matrices consisting of variances along the principal axes of each color distribution, which are given by the eigenvalues of the covariance matrices.

Next, the calculation of $\{\widetilde{\mathbf{I}'_j}\} = \mathbf{Q}_i^{-1}\{\mathbf{I}'_j\}$ decorrelates the data so that its covariance becomes an identity matrix: $\mathrm{cov}(\{\widetilde{\mathbf{I}'_j}\}) = \mathbf{Id}$. Then, the calculation of $\{\widehat{\mathbf{p}'_j}\} = \mathbf{R}_i\{\widetilde{\mathbf{I}'_j}\}$ reconstructs the data so that its covariance becomes the same as $\{\mathbf{p}_j\}$: $\mathrm{cov}(\{\widehat{\mathbf{p}'_j}\}) = \mathrm{cov}(\{\mathbf{p}'_j\})$. Thus the solution of $\mathbf{A}_i$ is given by

$$\mathbf{A}_i = \mathbf{R}_i\mathbf{Q}_i^{-1} = (\mathbf{V}_i\mathbf{\Xi}_i^{\frac{1}{2}})(\mathbf{\Sigma}_i^{-\frac{1}{2}}\mathbf{U}_i^T). \tag{8}$$

When substituting (6), (7), and (8) into (4), a zero matrix results: $\mathbf{R}_i\mathbf{Q}_i^{-1}(\mathbf{Q}_i\mathbf{Q}_i^T)\mathbf{Q}_i^{-T}\mathbf{R}_i^T - \mathbf{R}_i\mathbf{R}_i^T = \mathbf{0}$. However, there are several solutions for $\mathbf{A}_i$ since the order of the components of $\mathbf{R}_i$ and $\mathbf{Q}_i$ is arbitrary. Some solutions cause discolorations. A method to deal with this problem is described in Sec. 3.

2.3. Global color transformation

The local color transformation of each patch is assumed to be $\{\mathbf{A}_i\mathbf{I}_j + \mathbf{b}_i\}_{j\in\Omega_i}$, while the practical color transformation for the whole image is performed so as to obtain the optimal pixel colors $\mathbf{q}_i^*$ using all the computed values of $\mathbf{A}_i$ and $\mathbf{b}_i$ [1,2,4]. The energy function is defined as

$$\arg\min_{\mathbf{q}} \sum_i \sum_{j\in\Omega_i} w_{ij}\|\mathbf{A}_i\mathbf{I}_j + \mathbf{b}_i - \mathbf{q}_j\|_2^2. \tag{9}$$

When the weights are constant $w_{ij} = 1$, it corresponds to the standard GF [1]. The solution is given by

$$\mathbf{q}_i^* = \overline{\mathbf{A}}_i\mathbf{I}_i + \overline{\mathbf{b}}_i, \tag{10}$$

where $\overline{\mathbf{A}}_i = \frac{1}{N}\sum_{j\in\Omega_i}\mathbf{A}_j$ and $\overline{\mathbf{b}}_i = \frac{1}{N}\sum_{j\in\Omega_i}\mathbf{b}_j$ are mean values around pixel i, N is the number of pixels, and the weights are normalized so that $N = \sum_j w_{ij}$. When $w_{ij} \in \{0, 1\}$, a rough but fast calculation method is described in [3]. In other general cases, $\overline{\mathbf{A}}_i$ and $\overline{\mathbf{b}}_i$ are obtained by convolutional filtering of time-variant filters with coefficients w_{ij} and coefficient images that have $\mathbf{A}_i$ and $\mathbf{b}_i$ as their pixel values. For details, please refer to [4].

3. ANALYSIS AND REDUCTION OF DISCOLORATIONS

The color transform matrices $\mathbf{A}_i$ obtained in the preceding section have some drawbacks, and cause discolorations when being used for color transformation directly. In this section, we mention two problems that cause the discolorations, and describe a solution for the problem.

3.1. Correction of the order and signs of eigenvectors

Although a color transform matrix is given as the product of two matrices $\mathbf{U}_i$ and $\mathbf{V}_i$ composed of eigenvalues and eigenvectors as shown in (8), it has two *ambiguities*: (i) the order of the principal eigenvectors; (ii) the direction (sign) of the eigenvectors. The first problem arises from the fact that the color distribution of a uniform color region becomes spherical. Thus the order of the axes is easily switched due to the influence of noise, *e.g.*, $[\mathbf{u}_1|\mathbf{u}_2|\mathbf{u}_3] \rightarrow [\mathbf{u}_1|\mathbf{u}_3|\mathbf{u}_2]$. The second problem is that the signs of the eigenvectors are generally not specified. Thus there is a possibility of sign inversion in each column, *e.g.*, $[\mathbf{u}_1|\mathbf{u}_2|\mathbf{u}_3] \rightarrow [\pm\mathbf{u}_1|\pm\mathbf{u}_2|\pm\mathbf{u}_3]$. To address these problems, we assume the following:

- **Assumption 1**: A patch pair has similar color distribution shapes. Furthermore, the order of the principal axes is the same as that of the paired patch $\mathbf{u}_k \leftrightarrow \mathbf{v}_k$. Although the color distribution becomes spherical in a uniform color region and the order of the axes is undecidable, it matters little because, in such a region, the variance along each axis is similar
- **Assumption 2**: On the k'th axis, the two eigenvectors of a patch pair have the same orientation. The direction is corrected using the sign of the inner product: $\mathbf{u}_k := \mathbf{u}_k \cdot \mathrm{sign}(\mathbf{u}_k^T\mathbf{v}_k)$.

3.2. Correction for eigenvalues in $\mathbf{\Xi}_i$ and $\mathbf{\Sigma}_i$

The matrix $\mathbf{R}_i$ in $\mathbf{A}_i = \mathbf{R}_i\mathbf{Q}_i^{-1}$, *i.e.*, $\mathbf{R}_i = \mathbf{V}_i\mathbf{\Xi}_i^{\frac{1}{2}}$ is obtained from noisy data, and the influence of the noise mainly appears in $\mathbf{\Xi}_i$. That is, when a color distribution is stretched by the influence of noise, its variances given by diagonal values $\{\xi_1^2, \xi_2^2, \xi_3^2\}$ increase. This leads to an excessive expansion of the transformed color distribution, and discoloration emphasis. From our knowledge, the standard

(a) Guide image (b) Noisy input (c) Our previous GF [4] (d) Proposed GF

Fig. 1. Color and contrast transformation by GFs for dynamic and static regions. Top: results of the dynamic region. Bottom: results of the static region. From left to right, guide images with ideal sharpness but the incorrect contrast (a), noisy input images with ideal contrast (b) (additional noise with standard deviation 0.06 is added), and results of our previous GF (c) and proposed GF (d). The areas inside the red circles are deteriorated.

deviations along the 2nd and especially 3rd axes $\{\xi_2, \xi_3\}$ are linked to the discolorations. Even if original data do not include any noise, expanding the color distribution toward the 2nd and 3rd axes emphasizes the discolorations.

As mentioned above, causes of the discolorations are associated with the diagonal values of $\mathbf{\Xi}_i$, more specifically, the ratios of the diagonal elements $\mathbf{\Xi}_i^{\frac{1}{2}} \mathbf{\Sigma}_i^{-\frac{1}{2}} = \mathrm{diag}([\frac{\xi_1}{\sigma_1}, \frac{\xi_2}{\sigma_2}, \frac{\xi_3}{\sigma_3}])$ included in $\mathbf{R}_i \mathbf{Q}_i^{-1}$. To reduce discolorations, we restrict the diagonal values of $\mathbf{\Xi}_i$ by comparing them with those of $\mathbf{\Sigma}_i$ that do not include noise as follows:

- The 3rd eigenvalues are the main cause of discolorations. The smaller one is used: $\xi_3 := \min(\xi_3, \sigma_3)$, *i.e.*, $\frac{\xi_3}{\sigma_3} \leq 1$;
- The 2nd eigenvalues are replaced with those obtained from data without noise: $\xi_2 := \sigma_2$, *i.e.*, $\frac{\xi_2}{\sigma_2} = 1$;
- The 1st eigenvalues are used without any correction.

4. CLASSIFICATION OF STATIC / DYNAMIC REGIONS AND BLENDING METHOD OF GUIDED FILTERS

As a result of the GFs described in the previous sections, Fig. 1 shows the resulting images of our previous GF [4] for static regions (c) and proposed GF for dynamic regions (d). As can be seen in (d), the proposed GF yields a natural image without blur for the dynamic region, while it unfortunately yields discolorations for the static region due to the noise in the input image. Since each method has advantages and disadvantages, we aim to use an appropriate GF selectively region-by-region so as to obtain more natural results.

We find that the blur artifacts of existing GFs are associated with the norms of the transform matrices $\|\mathbf{A}_i\|$, *i.e.*, they play the role of a scaling factor for the contrast of each patch, and as they decrease, the value of $\mathbf{A}_i \mathbf{I}_j$ becomes closer to $\mathbf{0}$. Thus the result approaches the mean colors of the patches $\mathbf{A}_i \mathbf{I}_j + \mathbf{b}_i$ to $\mathbf{b}_i$. However, this also indicates that the dynamic regions can be classified by observing the norms and transformation errors of (1). Thus we classify the static and the dynamic regions by using the *support vector machine* (SVM) [11, 12] [2]. The SVM is performed using a training phase and a test phase. The details of the training phase are described in the next section. The results of the test phase are shown in Sec. 5.

4.1. SVM Training and Image feature vector

For the SVM training, we use the multiple image sets shown in Fig. 2: (a) and (b) are guide and input images, and (c) is a scribble image to specify static regions (black scribbles) and dynamic

(a) Guide image (b) Input (c) Scribble

Fig. 2. Sample sets of images used in the SVM traning phase.

regions (white scribbles). We define pixel labels for the static regions as ($y_i = -1$) and the dynamic regions as ($y_i = +1$). The gray regions in (c) are not used. Then we define feature vectors ($\in R^3$) for classifying the labels as follows:

- Frobenius norm of a transform matrix $\|\mathbf{A}_i\|_F^2 \in R^1$;
- l_2 norm of an offset vector $\|\mathbf{b}_i\|_2^2 \in R^1$;
- Error of fidelity term: $\sum_{j \in \Omega_i} w_{ij} \|\mathbf{A}_i \mathbf{I}_j + \mathbf{b}_i - \mathbf{p}_j\|_2^2 \in R^1$.

These three scalar values are bundled as a feature vector for each pixel. The second feature is intended for discolorations occurring in dark regions where $\|\mathbf{b}\| \approx 0$ and the shapes of color distributions become spherical. Using these labels and feature vectors, the SVM training is performed.

4.2. Classification and Blending methods

When the labeling is done as described above, the classification results y_i of the dynamic regions are given as positive values ($y_i > 0$), while those of the static regions are given as negative values ($y_i < 0$). The proposed GF is applied to pixels classified as dynamic regions, and the $\mathbf{A}_i$ matrices are recalculated ($\mathbf{b}_i$ are shared with all the regions).

To this end, we simply blend the resulting images of the conventional GF $\mathbf{q}_i$ and proposed GF $\mathbf{q}'_i$ by pixel-wise blending:

$$\mathbf{q}_i^* = (1 - \alpha(y_i))\, \mathbf{q}_i + \alpha(y_i)\, \mathbf{q}'_i, \tag{11}$$

where $\alpha(y_i) \in [0, 1]$ denotes a blending coefficient defined on the basis of the pixel label y_i. As for the function $\alpha(\cdot)$, for example, sigmoid functions such as $\alpha(y_i) = (1 + \exp(-\beta y_i))^{-1} \in [0, 1]$ are available, where β is a parameter to control the transition width. The experimental results using this blending method are shown in Sec. 5.

[2] In the implementation, we use the SVM-light [13] with a radial basis function kernel [11, 12], and simply use default parameters.

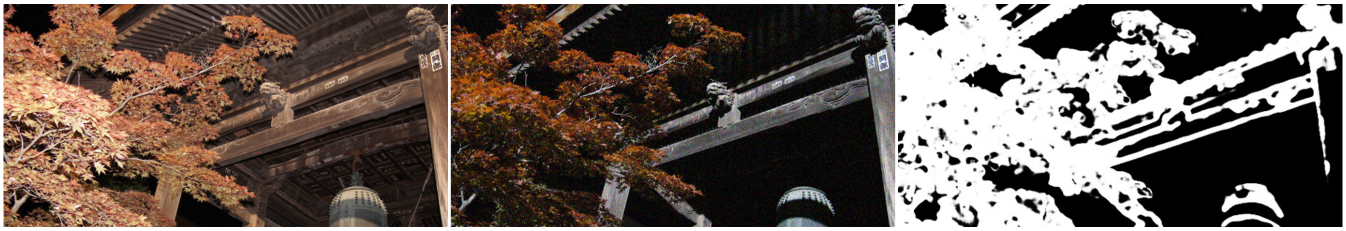

(a) Guide image (b) Noisy input (c) Classified

Fig. 3. Results of the SVM test phase. Using the image pair (a) and (b), the SVM automatically outputs (c).

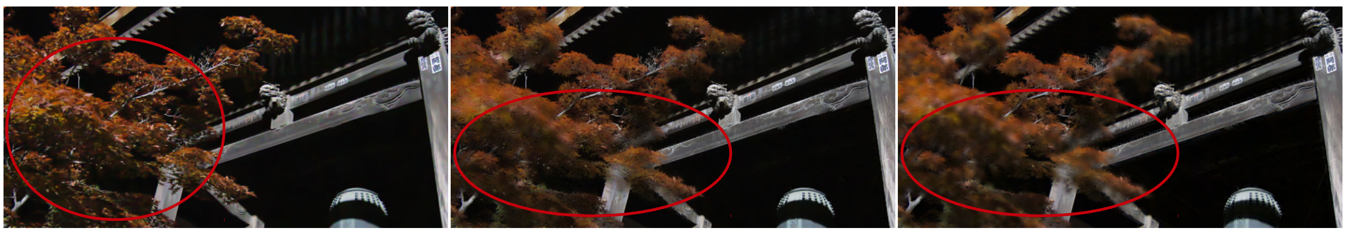

(a) BM3D [14] (b) Joint bilateral filtering [15] (c) GF [1]

(d) Our previous GF (e) Proposed GF (f) Blended GF

Fig. 4. Results of flash / no-flash image integration, *i.e.*, denoising of a no-flash image. Top: results of standard methods. Bottom: results of our methods. The area inside each red circle is deteriorated.

5. EXPERIMENTAL RESULTS

To validate the performance of SVM classification and blending using (11), we performed the SVM test phase and show the resulting images. As an application, we chose the *flash / no-flash image composition* (denoising of a no-flash image), with the use of GFs (this application was originally proposed in [15, 16]) because the flash (guide) image and the no-flash (noisy input) image include many bad correspondences caused by under / over-exposures in areas other than the dynamic regions. As for the images, intensities were normalized to the range $[0, 1]$, and this test phase was performed by using a noisy input image with additional Gaussian noise (standard deviation is 0.06).

Fig. 3 shows a result of classification by SVM. The dynamic regions in the image pair (a) and (b) are automatically classified as shown in (c), where (c) indicates a coefficient map $\alpha(y_i)$ in (11), and static regions are displayed in black ($\alpha(y_i) = 0$), while dynamic regions are displayed in white ($\alpha(y_i) = 1$).

Fig. 4 shows a comparison of our proposed GF and blended GF with standard methods [1, 14, 15], and our conventional GF [4]. Each method is prone to produce some artifacts on the leaves of the maple tree. The BM3D [14] is shown here as a representative denoising method for a single image (a). It however causes unnatural patterns on the resulting images. From the original method of this application [15] (b) and the standard GF [1] (c), similar results are obtained and their dynamic regions suffer from blur artifacts. This is mainly caused by the pixel misalignment of the dynamic regions. On the other hand, our previous GF, *i.e.*, weighted GF, reduces the blur artifacts but still leaves discoloration artifacts. The proposed GF gives good results except for discoloration artifacts in the dark regions. The final result (f) yielded by blending (d) and (e) has a natural appearance. The main improvement is a decrease in the discoloration artifacts, for example, the above mentioned dark regions of (f) are replaced by those of (d).

The classification performance of the SVM shown in Fig. 3 (c) is actually thought to be a little excessive since some static regions are incorrectly detected (*e.g.*, beams of the bell house). However, using similar sets of image pairs in the training phase, the accuracy is improved. This problem is similar to image matting [8, 17] especially to the latter method. That is, giving sample labels to partial regions as scribbles or trimap, the other regions are automatically labeled. Therefore the techniques developed in image matting may be useful to improve the classification accuracy.

6. CONCLUSION

We presented a GF for dynamic regions and a method to classify static / dynamic regions. Instead of using pixel-to-pixel correspondences, our method introduces correspondences of local covariance matrices. In classification, we employed a support vector machine and used numerical values obtained from equations as a feature vector. The combination of GFs can yield images with less artifacts. In future work, blending and combining methods of GF equations will be considered in order to further reduce artifacts.

7. REFERENCES

[1] K. He, J. Sun, and X. Tang, "Guided image filtering," *IEEE TPAMI (Proc. ECCV 2010)*, vol. 35, no. 6, pp. 1397–1409, 2013.

[2] K. Shirai, M. Ikehara, and M. Okamoto, "Color and shadow replacing of flash and no-flash photos to create noiseless images," *IEICE T. Fundamental (Japanese) (Proc. IEEE ICIP 2011)*, vol. J94-A, no. 4, pp. 275–284, 2011.

[3] J. Lu, K. Shi, D. Min, L. Lin, and M. N. Do, "Cross-based local multipoint filtering," in *Proc. IEEE CVPR*, 2012, pp. 430–437.

[4] K. Iwata, K. Shirai, and M. Okuda, "Local color distribution projection filtering using a homogeneous coordinate system," in *Proc. IEEE ICIP*, 2013.

[5] L. Yuan and J. Sun, "Automatic exposure correction of consumer photographs," in *Proc. ECCV*, 2012, pp. 771–785.

[6] C. Rhemann, A. Hosni, M. Bleyer, C. Rother, and M. Gelautz, "Fast cost-volume filtering for visual correspondence and beyond," *IEEE TPAMI (Proc. CVPR 2011)*, vol. 35, no. 2, pp. 504–511, 2013.

[7] I. Omer and M. Werman, "Color lines: Image specific color representation," in *Proc. IEEE CVPR*, 2004, vol. 2, pp. 946–953.

[8] A. Levin, D. Lischinski, and Y. Weiss, "A closed-form solution to natural image matting," *IEEE TPAMI (Proc. CVPR 2006)*, vol. 30, no. 2, pp. 228–242, 2008.

[9] Q. Shan, J. Jia, and M.S. Brown, "Globally optimized linear windowed tone mapping," *IEEE T. Visualization Comput. Graph.*, vol. 16, no. 4, pp. 663–675, 2010.

[10] A. Bousseau, S. Paris, and F. Durand, "User-assisted intrinsic images," *ACM TOG (Proc. SIGGRAPH Asia)*, vol. 28, no. 5, pp. 130:1–130:10, 2009.

[11] C. Cortes and V. N. Vapnik, "Support-vector networks," *Machine Learning*, vol. 20, pp. 273–297, 1995.

[12] C. J. C. Burges, "A tutorial on support vector machines for pattern recognition," *Data Mining and Knowledge Discovery*, vol. 2, pp. 121–167, 1998.

[13] T. Joachims, *Learning to classify text using support vector machines*, Kluwer, 2002.

[14] K. Dabov, A. Foi, V. Katkovnik, and K. Egiazarian, "Image denoising by sparse 3D transform-domain collaborative filtering," *IEEE Trans. Image Process.*, vol. 16, no. 8, pp. 2080–2095, 2007.

[15] G. Petschnigg, R. Szeliski, M. Agrawala, M. Cohen, H. Hoppe, and K. Toyama, "Digital photography with flash and no-flash image pairs," *ACM Trans. Graph. (Proc. SIGGRAPH)*, vol. 23, no. 3, pp. 664–672, 2004.

[16] E. Eisemann, E. Eisemann, and F. Durand, "Flash photography enhancement via intrinsic relighting," *ACM Trans. Graph. (Proc. SIGGRAPH)*, vol. 23, no. 3, pp. 673–678, 2004.

[17] Y. Li, E. Adelson, and A. Agarwala, "ScribbleBoost: adding classification to edge-aware interpolation of local image and video adjustments," in *Proc. Eurographics Conf. Rendering*, 2008, pp. 1255–1264.